Journal of Power Sources 190 (2009) 493–498

Contents lists available at ScienceDirect

Journal of Power Sources

journal homepage: www.elsevier.com/locate/jpowsour

Visualization of unstable water flow in a fuel cell gas diffusion layer

Bin Gao[a,b], Tammo S. Steenhuis[a,*], Yunati Zevi[a], J.-Yves Parlange[a], Robert N. Carter[c], Thomas A. Trabold[c]

[a] Biological & Environmental Engineering, Cornell University, Ithaca, NY 14853, United States
[b] Agricultural and Biological Engineering, University of Florida, Gainesville, FL 32611, United States
[c] General Motors Corporation, Fuel Cell Research Laboratory, Honeoye Falls, NY 14472, United States

ARTICLE INFO

Article history:
Received 2 December 2008
Received in revised form
28 December 2008
Accepted 30 December 2008
Available online 14 January 2009

Keywords:
Water transport
Unstable flow
GDL
PEM fuel cell
Visualization
Capillary pressure

ABSTRACT

Modeling two-phase flow in proton exchange membrane (PEM) fuel cells is hampered by a lack of conceptual understanding of flow patterns in the gas diffusion layer (GDL). In this paper, pore-scale visualizations of water in different types of GDLs were used to improve current understanding of flow and transport phenomena in PEM fuel cells. Confocal microscopy was used to capture the real-time transport of water, and pressure micro-transducers were installed to measure water breakthrough pressures. Three types of fuel cell GDLs were examined: TO series (Toray Corp., Tokyo, Japan), SGL series (SGL Carbon Group, Wiesbaden, Germany), and MRC series (Mitsubishi Rayon Corp., Otake City, Japan). The visualizations and pressure measurements revealed that despite difference in "pore" structures in the three types of GDLs, water followed distinct flow paths spanning several pores with characteristics similar to the "column flow" phenomena observed previously in hydrophobic or coarse-grained hydrophilic soils. The results obtained from this study can aid in the construction of theories and models for optimizing water management in fuel cells.

© 2009 Elsevier B.V. All rights reserved.

1. Introduction

Achieving maximum power density, a key objective for proton exchange membrane (PEM) fuel cells research [1,2], requires unrestricted transport of oxygen and hydrogen from gas channels to the catalyst layers [3–6]. Increased power, however, generates significant product water [7–12], which may block pores in the gas diffusion layer (GDL) and restrict the transport of reaction gases [13]. Because understanding of water transport and removal in fuel cell GDL is limited but crucial to increased power generation, these processes need to be further studied to facilitate the commercial application of fuel cells [4,14,15].

To explore water flow in PEM fuel cells, various techniques have been employed to visualize water in GDL and flow channels [8,12,13]. Yang et al. [16] and Zhang et al. [8] were able to visualize with an optical microscope the emergence of water droplets at specific locations from the GDL surface and its subsequent transport into flow channels in a transparent fuel cell fixture. Employing neutron tomography, Pekula et al. [17] found under real operating conditions accumulation of water at specific locations within the fuel cell. Kramer et al. [18] showed with neutron radiography that a serpentine flow channel was the most effective in removing the emerging water from a GDL. Litster et al. [13] successfully used a fluorescence microscopy technique to visualize liquid flow as it emerged from the surface and a few micrometers below the surface of a GDL. They suggested that water transport was dominated by "fingering and channeling" through individual pores. However, the finger (or column) flow phenomena in GDL as suggested by Litster et al. [13] have not been studied well in fuel cell research.

In addition to visualization studies, numerical and analytical models have been used to optimize fuel cell designs by simulating reactant fluid flow [19–23]. These models range from simplistic single-phase water or vapor transport models to complicated two-phase models combining both the Darcy's and diffusion laws. The ability of current models to simulate two-phase flow and water management in PEM fuel cells was addressed by Weber and Newman [5], Schulz et al. [20], and Wang [6]. These authors indicated that current models are plagued by the scarcity of realistic conceptualization of the interactions between water and GDL. Visualizations of water dynamics within GDL, such as images revealing both water and the GDL, can be used to inform the conceptualization of these models.

Early visualization studies suggested that water transport in GDL is unstable [13], which is similar to the column flow phenomenon occurring in natural porous media. The column flow can be found both in coarse-grained hydrophilic [24–27] and natural hydrophobic porous media [28,29]. Theories developed for natural porous

* Corresponding author at: Riley-Robb Hall, Cornell University, Ithaca, NY 14853, United States. Tel.: +1 607 255 2489; fax: +1 607 255 4080.
E-mail address: tss1@cornell.edu (T.S. Steenhuis).

0378-7753/$ – see front matter © 2009 Elsevier B.V. All rights reserved.
doi:10.1016/j.jpowsour.2008.12.135

media showed that column flow is an unstable phenomenon in which water enters the porous media at regular spaced points. Depending on the imposed flow rate one or more of these "entrance points" result in finger like structure. Unlike the idea of Litster et al. [13] that column flow is restricted to a single pore, in naturally occurring porous media it spans from several to hundreds of pore diameters.

It is unclear whether the column flow theory for naturally occurring porous media can be applied to fuel cells in which the GDL is made of fibers with different shapes and has much smaller pores than those of the typical hydrophobic soils. Additional studies, especially experimental investigations, are needed to improve the fundamental understandings of the dynamics of water flow in fuel cell GDL. Our overall objective of this study is to better characterize the unstable water flow within PEM fuel cell GDL. Confocal microscopy was used to visualize the real-time transport of water within different types of GDLs. The visualizations together with water transport pressure measurements indicate that the unstable column flow phenomena in the GDL are similar to those in soil porous media, which are studied intensively with well-established theories and models. The findings from this study can inform the conceptualization and refinement of mathematical models of water transport and management in PEM fuel cells.

2. Materials and methods

2.1. Confocal microscopy

A confocal microscope was used to visualize liquid water in different types of PEM fuel cell GDLs. Confocal microscopy is a modification of fluorescence microscopy that optically sections a specimen using small apertures (which are confocal) to eliminate out of focus and background signals. Different depths of focus can be obtained with a precise Z-stepping stage. The instrument can record simultaneously four different signals (or spectral channels). In our application, a confocal Leica TCS SP2 microscope was used that can detect fluorescing objects of approximately 0.5 μm. Two of the four spectral channels were employed: one for detecting the fibers (excited at 488 nm), another to detect the water stained with Rhodamine B (excited at 543 nm). Overlays of the two channels made it possible to view fibers and water in the same image either as a series of still images of horizontal planes through the GDL (0.5 s minimum time step) or as quasi 3-D images by composition of single images taken along the z-axis at an interval of 1 μm.

2.2. Gas diffusion layer

Three types of GDLs with various thicknesses and percentages of polytetrafluoroethylene (PTFE) coating were studied: TO series (Toray Corp., Tokyo, Japan), SGL series (SGL Carbon Group, Wiesbaden, Germany), and MRC series (Mitsubishi Rayon Corp., Otake City, Japan) (Table 1). All these GDLs are carbon fiber papers coated with PTFE to render them hydrophobic. The TO series had five different GDLs ranking from the thinnest to thickest: TO30, TO60, TO90, TO120, and TO1.0. According to the manufacturer, the TO30 consists of one layer of carbon paper of approximately 120 μm thickness. The TO60, TO90, and TO120 have two or more layers of carbon papers that have been fused together. The TO1.0 GDL is a one layer thick carbon paper of about 1 mm. The SGL series consists of two types of GDLs: SGL25AA and SGL100AA, having similar surface properties. The MRC series also has two types: MRC104 and MRC107, which are similar to each other. The thickness of each GDL is given in Table 1. The GDLs were cut in 2 cm by 3.5 cm pieces for the pore-scale visualization studies. In order to facilitate locating the point of the breakthrough of the liquid for visualization purposes, a Kapton film (3 M) with small pore (100 μm) at the center was glued in some experiments on one side of the diffusion layer.

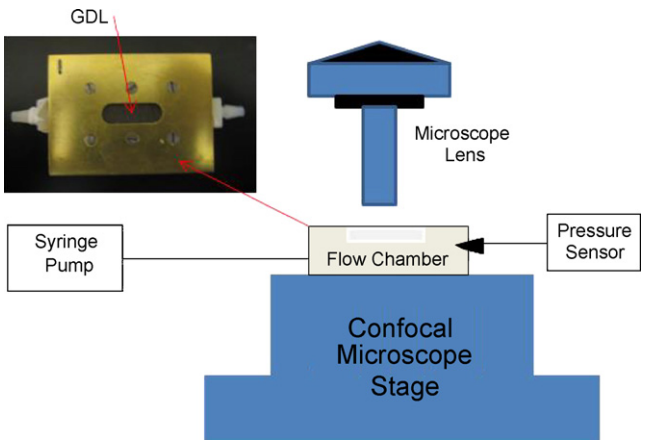

Fig. 1. Experimental setup for water transport in gas diffusion layer.

2.3. Flow system

Flow chambers with dimensions of 5.1 cm by 3.8 cm by 1.5 cm were used (Fig. 1). The flow chamber is made of brass and consists of two pieces. The bottom piece is 12 mm thick and has a small reservoir of 1.8 cm^3 etched inside. There are two-side openings in the bottom piece: one for connecting to a syringe pump and the other to a pressure sensor. The top piece is 2 mm thick and has an opening of 1.8 cm^2 for visualization of the water movement (Fig. 1). To prevent leakage, the GDL was sandwiched with silicone glue between the top and bottom pieces, which were clamped together using six screws.

Low power, non-amplified, non-compensated Honeywell 26PC Series micro-pressure sensors measured capillary water pressures during the visualizations (Fig. 1). The voltage output signal was amplified to a range of 10×, 100×, or 1000× and stored in a USB-based DAQ module with speed as high as 48 kS s^{-1}.

Table 1
Breakthrough pressures and finger sizes of water transport in diffusion layer.

Name	Thickness (μm)	PTFE (% wt)	P_b no film (Pa)	P_b with film (Pa)	Water column size (μm)[a]
TO30	100	7.8	60–200	450–500	130–740
TO60	190	5.2	70–450	300–700	170–700
TO90	280	4.8	450–700	800–1200	110–280
TO120	400	4.3	550–800	1200–1700	70–300
TO1.0	980	4.6	150–700	80–650	50–320
SGL25AA	190	10.5	30–200	150–500	120–730
SGL100AA	100	9.6	60–200	300–700	180–500
MRC104	120	10.0	300–340	120–520	180–730
MRC107	210	8.75	120–300	160–650	160–580

[a] Measured from the wet images (e.g. Fig. 5).

2.4. Experimental methods

A day before each experiment the GDL was sandwiched between the bottom and top pieces of the experimental flow chamber. Then the chamber was placed under the objective lens of the Leica confocal microscope (Fig. 1). The micro-pressure transducer and a syringe pump were connected to the flow chamber. The real-time visualization experiment was started by pumping fluorescent dyed water into the reservoir at the bottom piece of the flow chamber at a flow rate of 0.0027 mL min^{-1} cm^{-2}, which corresponds to an operation current density of 0.48 A cm^{-2}. The flow rate is within the range of the water fluxes generated in operating PEM fuel cells. Once the reservoir was full, and water broke through the GDL, the pump was stopped and any excess water droplet on the GDL surface was removed. In cases where the confocal microscope did not capture the breakthrough, the lens of the microscope was moved to the water breakthrough point. After the focal plane was identified, the pump was started again for another breakthrough experiment. This experimental procedure was repeated several times. During the water application, images of water transport within the GDL were taken through the confocal microscope with two different laser scanning speeds: 400 Hz and 1000 Hz. At the two laser scanning speeds, the confocal microscope can take images of water in the GDL as fast as 1 s per image and 0.4 s per image, respectively.

In addition to the real-time transport images, a three-dimensional image of the dry GDL was taken before the water was pumped into the flow chamber and after the water breakthrough of the wet GDL. In order to make three-dimensional images, the objective lens of the confocal microscope was set to do the step-move with equal distance (1.5 μm) along the vertical direction to visualize different images of the GDL at single focal planes (Z-step scanning) up to a depth of 150 μm. Then single slice images were composed into a three-dimensional image using Leica Confocal Software provided with the microscope. For all the images the 10× objective lens was used because it had sufficient working distance.

3. Results

3.1. Visualizations

The maximum depth that the confocal microscope could clearly distinguish the fibers in various GDLs varied between 80 and 130 μm (Fig. 2). We found the addition of Kapton film to the GDL did not affect the visualization depth. Most of the TO series (T030, TO60, TO90, and TO120) show large values of the visualization depth (110–130 μm); however, the TO1.0 GDL has the smallest depth (80 μm). For the MR series GDLs, the confocal microscope could distinguish fibers to a depth of around 110 μm. The SGL series GDLs had a slightly smaller visualization depth of approximately 95 μm.

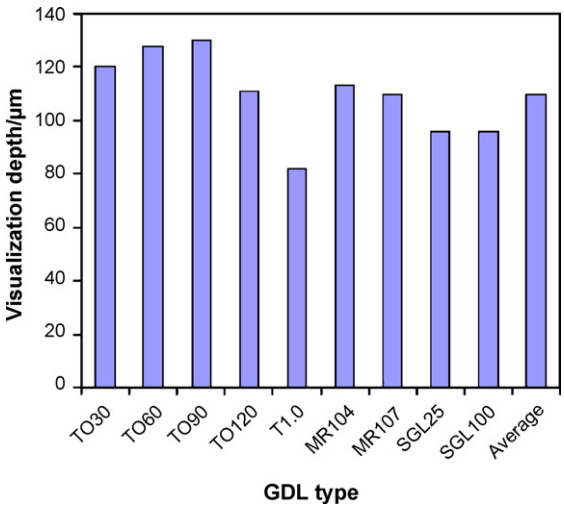

Fig. 2. Visualization depths of different gas diffusion layers.

Three-dimensional visualizations composed of single images taken at sequential focal planes with a 1.5 μm step within the GDLs at dry condition show no notable difference up to the maximum visualization depth, and therefore only one GDL of each type is depicted in Fig. 3. In addition, a close examination of the 3-D images indicates that the TO and MR series (Fig. 3a and b) are similar with a uniformly distributed fiber network and with an average pore opening of around 30 μm. The pores of SGL series are not uniformly distributed (Fig. 3c), and have many large pores with diameter around 80 μm, which is more than twice the pore size of TO and MR series.

Dynamics of the water movement in the GDLs were captured by confocal microscopy as real-time videos. During the visualization, the objective lens of the confocal microscope was focused at a distance of about 50 μm from the GDL surface. Fig. 4 shows selected still images of water transport in TO60 diffusion layer to illustrate the typical breakthrough pattern. The video, TO60n.wmv, itself is available at http://www.abe.ufl.edu/~bingao/videos.htm. Videos from some of the other studied GDLs are shown as well. In Fig. 4 and the corresponding video, water appears as red spots surrounded by dark green fibers. The still image sequences show that water breakthrough in GDL is fast, occurring within several seconds of first observing liquid water in the GDL. During the breakthrough, water only moved out from a small spot in the GDL as an unstable column flow. The image snapshots from the video in Fig. 4 show water breakthrough from upper left of the GDL image as a droplet at $t = 32.8$ s with a diameter spanning at least four fibers. In addition to the exit point in the upper left corner, water can be seen in some locations near the breakthrough point. Water in those loca-

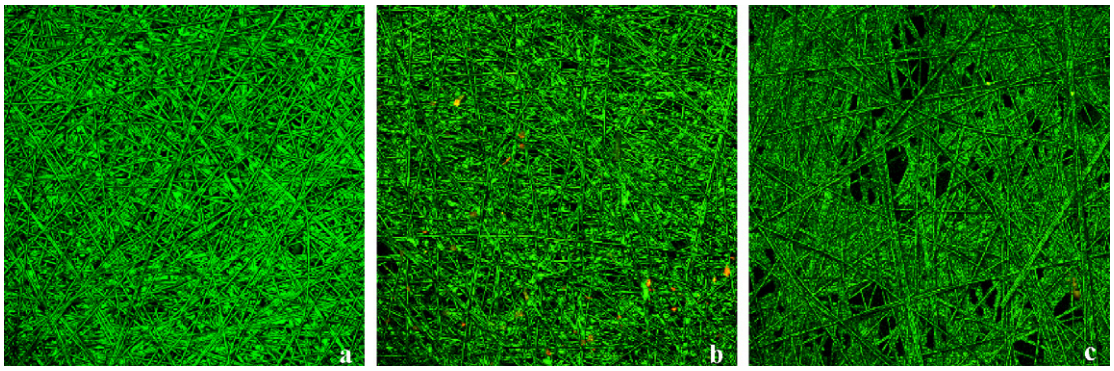

Fig. 3. Visualization examples of dry gas diffusion layers with 1.5 mm × 1.5 mm field of view: (a) TO30, (b) MR104, and (c) SGL25AA.

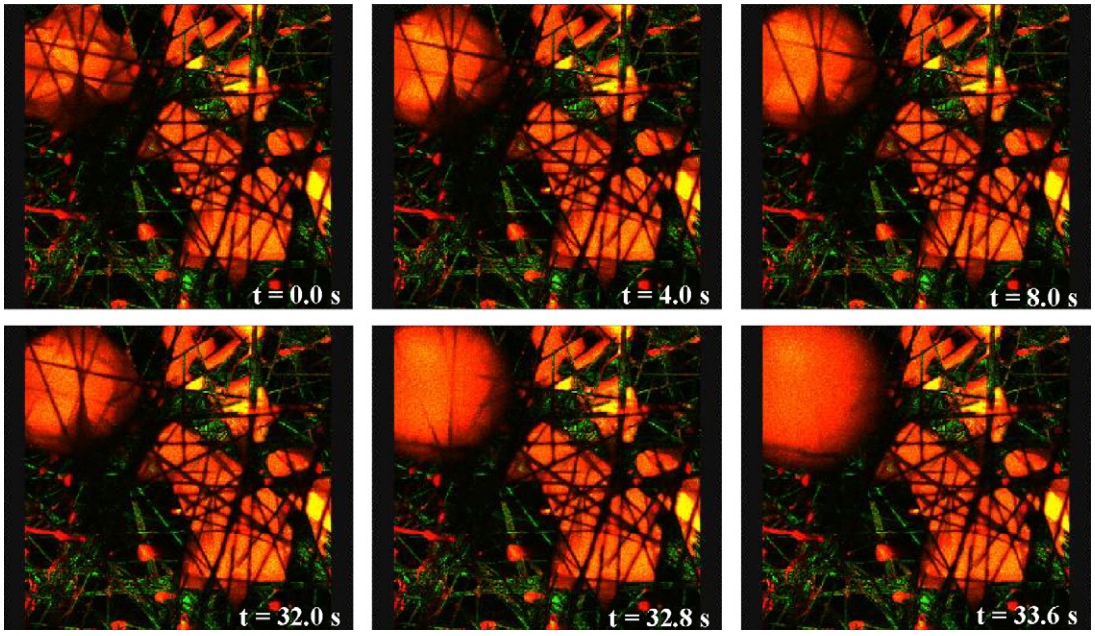

Fig. 4. Real-time visualization of water transport in TO60 with 0.75 mm × 0.75 mm field of view.

tions does not move in a straight path and appears much deeper in the GDL as several fibers can be seen in front of it. Before the sudden breakthrough (from $t = 32$ s), water accumulates and moves sideways (in-plane) to the breakthrough point from different locations (Fig. 4).

Due to the fast changing flow pattern, the dynamic water movement could only be recorded at one confocal plane. Fig. 5 shows examples of 3-D images of water in the three different GDLs, which were taken after the water flow was stopped. Similar to the "dry images" in Fig. 2, these "wet images" are also composed of single images at different focal planes. Water is observed as yellow–red fluorescent spots in the green diffusion layer and occupies a relatively small area spanning several pores. These spots are not uniformly distributed in the GDLs. For all the diffusion layers, the sizes of the water columns varied among different diffusion layer samples. The diameters of these water columns have wide ranges with values between 50 μm and 740 μm (Table 1).

3.2. Pressure measurements

A large variation in the breakthrough pressures (30–1700 Pa) was observed for different types of GDLs (Table 1). In general, GDL with a Kapton film has much larger breakthrough pressures than GDL without the film, except for the T1.0 series. However, there is no clear pattern that can relate breakthrough pressures of the GDLs with their thicknesses, PTFE percentages, or water column sizes.

The water breakthrough pressure was measured several times for each of the GDL flow chambers by stopping and restarting the pump. There were slight pressure changes for water transport through the same GDL at different runs. For all of the GDLs tested in this study, we found that the breakthrough pressure was always highest at the first run (i.e. water through dry GDL) and decreased with successive runs. Fig. 6 shows an example of pressure changes in a TO60 GDL with three water-breakthrough tests. Initially, after water filled the visualization chamber, water pressure rose slowly as the GDL sandwiched between the plates in the chamber stretched and deformed. Once the GDL could not deform further, the pressure increased dramatically in a very short time. When the water pressure reached the dry breakthrough point (~660 Pa), water broke through the porous media and the pressure dropped immediately (at approximately 120 s in Fig. 6). The pressure then decreased slowly after the pump was stopped. When the second water-breakthrough test started, water pressure increased quickly again to reach the wet breakthrough point (~560 Pa), which is lower than that of the dry test. The breakthrough pressure of the third test (~550 Pa) is slightly lower that of the second test. These results suggest that wetting history of the GDL may play an important role in controlling water transport.

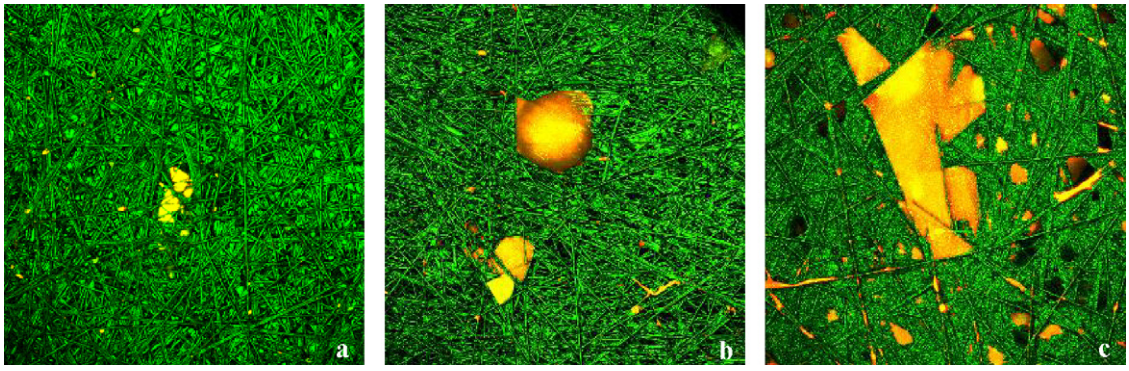

Fig. 5. Visualization examples of wet GDLs with 1.5 mm × 1.5 mm field of view: (a) TO30, (b) MR104, and (c) SGL100AA.

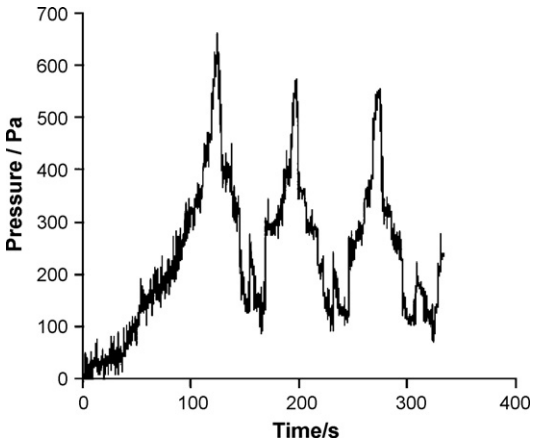

Fig. 6. Real-time breakthrough pressure of water transport in TO60 during three, consecutive breakthrough events.

4. Discussion

In the visualization study, all the tested GDLs show preferential flow despite that the properties of the three GDLs are different (Table 1). In no experiment did a GDL sample become fully saturated, and the sizes of water columns vary with different types of GDLs but are all smaller than 1 mm (Table 1). To find out whether the column flow in the GDL is similar to that observed in soils (hydrophobic and coarse-grained hydrophilic), we consider a sequence of images of water transport in the SGL100 GDL without Kapton film (Fig. 7). In this sequence, the lens of the confocal microscope happened to be placed at a position where it did not line up with the breakthrough point of water through SGL 100. When water filled up the flow chamber, the wetting front appeared after 32 s in the GDL at five distinct areas, each of these areas has a size of approximately 0.1 mm^2 within the 0.75 mm by 0.75 mm observation plane (Fig. 7). All of the five distinct areas in Fig. 7 could be the paths for the column flow. At 56 s, however, water broke through at another location outside the field of observation. All the water fronts in the images then suddenly disappeared (t = 56 s). This indicates that water breakthrough decreases the pressure and withdraws water from the pores (except water in the column flow) in the GDL. This phenomenon is similar to the unstable column flows observed in hydrophobic soils, although the scales are very different. When water is applied to hydrophobic soils, the wetting front also progresses at many locations in the porous media until one column gets far enough ahead of the others. The water pressure in hydrophobic soils also decreases behind the wetting front; however, the water in other locations may not withdraw as in the GDL because gravity can hold the water in the soil pores. In addition, when rewetting a GDL, the water follows the same path established during the first wetting cycle. At the same time, the pressure for subsequent breakthrough is smaller at the column tip in GDL (Fig. 6). These phenomena are very common in soils. Glass et al. [26] showed that the column flow in soils always establishes the same flow path on rewetting. Selker et al. [30] and Liu et al. [31] found that the pressure decreased in the column flow in soil after subsequent infiltrations. These phenomena can be explained by the hysteretic nature of the capillary pressure–moisture content relationship [26,32]. It is clear that unstable flow observed in hydrophobic (and coarse-grained hydrophilic) soils and in GDLs have many similarities and the water exiting the GDL surface in fuel cells are likely cause by unstable column flow.

The large spread in breakthrough pressures for the same GDL (Table 1) is also a result of the unstable flow phenomenon. As noted above, the water in the column breaks through the GDL when the water entry value is exceeded. The water entry pressure for the GDL should be the same if the material is uniform; however, the PTFE coated GDL is highly heterogeneous in hydrophobicity and pore sizes. Therefore, water in the GDL will try to break through from a location where it has the lowest entry pressure (i.e. large pore size with low hydrophobicity). In the cases when the sample is covered with Kapton film, water can only enter the GDL through a very small hole with limited access to the low entry pressure pores. As a result, the water breakthrough pressure of GDLs with film is much greater than that of GDLs without film (Table 1).

Many models of water transport in fuel cells assume that flow in GDLs is uniform and stable, and the governing equations can be solved in one dimension. However, both the visualizations and pressure measurements suggest that flow in GDLs varies in three dimensions. Thus in general, one-dimensional solutions of mass, momentum, and energy conservation equations should be applied with great care to fuel cell models because they are only valid to the

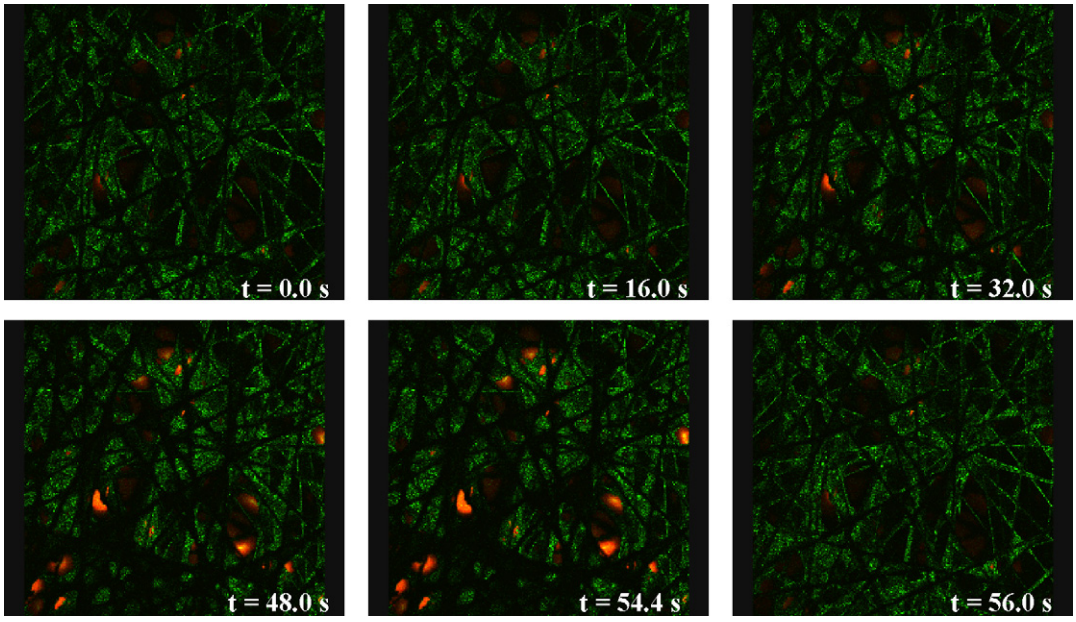

Fig. 7. Real-time visualization of water transport in SGL100 with 0.75 mm × 0.75 mm field of view.

column flow phenomena in special cases. Because unstable water flow in the fuel cell GDLs is similar to the column flow in soils, it may affect how water transport in GDLs should be modeled.

Predicting unstable column flow phenomena in Hele-Shaw cells and soils has drawn much attention of mathematicians and modelers since its early discovery [30,33]. The Saffman and Taylor's solution is likely the most famous model of the column flow in soils [34]. Parlange and Hill [27] developed the first analytical solution for predicting column sizes in soils. A later analytical model developed by Selker et al. [30,35] can accurately simulate the moisture and pressure profiles behind the finger tips of the columns flow. In their numerical studies of column flow in soils, Nieber et al. [36] found that the numerical models require the constitutive relationship (soil characteristic curves) to be hysteretic by having higher moisture content during drying than during wetting at a same matric or pressure potential. In addition to large-scale simulations, pore-scale models are also used with some successes to predict column flow in soils [37].

Because of the similarities of the column flow between fuel GDLs and soils, column flow models developed for soils can provide guidance to the development of fuel cell models in hysteresis analysis, diffusion characterization [32,38], quantification of interaction between contact angle and fingering [25], and analysis of finger widths [27]. However, notable differences exist between GDLs and soils, particularly with respect to the length scale and the pore characteristics. Despite the difficulties, developing new modeling approaches for water in GDLs is a must, because most current models use a non-hysteretic constitutive relationship and cannot predict the column flow behavior as observed in our and other experiments of water transport through GDLs in PEM fuel cells.

5. Conclusions

A novel, laser-scanning, confocal microscope technique was used to show the transport behavior of liquid water in GDLs. For the visualization purpose, fluorescent Rhodamine B dyed water was pumped through different fuel cell GDLs sealed in a flow chamber placed under the confocal microscope. Micro-pressure transducers were used in the experiment to monitor the pressure of water in the GDLs. Based on the pore-scale visualizations, we found that water flow in PEM fuel cell GDLs is unstable and similar to the column flows as commonly observed in hydrophobic soils. The pore-scale visualization system developed in this study can be used to explore the governing mechanisms of water transport that in turn can be used to inform the development of models optimizing water management in PEM fuel cells.

References

[1] Y.H. Cai, J. Hu, H.P. Ma, B.L. Yi, H.M. Zhang, Journal of Power Sources 161 (2006) 843–848.
[2] J.T. Gostick, M.W. Fowler, M.D. Pritzker, M.A. Ioannidis, L.M. Behra, Journal of Power Sources 162 (2006) 228–238.
[3] A.Z. Weber, R.M. Darling, Journal of Power Sources 168 (2007) 191–199.
[4] H. Ju, G. Luo, C.Y. Wang, Journal of the Electrochemical Society 154 (2007) B218–B228.
[5] A.Z. Weber, J. Newman, Chemical Reviews 104 (2004) 4679–4726.
[6] C.Y. Wang, Chemical Reviews 104 (2004) 4727–4765.
[7] S. Gottesfeld, Electrolyte Fuel Cells, Wiley–VCH, New York, 2007, pp. 195–301.
[8] F.Y. Zhang, X.G. Yang, C.Y. Wang, Journal of the Electrochemical Society 153 (2006) A225–A232.
[9] P.K. Sinha, P. Halleck, C.Y. Wang, Electrochemical and Solid State Letters 9 (2006) A344–A348.
[10] E.C. Kumbur, K.V. Sharp, M.M. Mench, Journal of Power Sources 161 (2006) 333–345.
[11] J.J. Kowal, A. Turhan, K. Heller, J. Brenizer, M.M. Mench, Journal of the Electrochemical Society 153 (2006) A1971–A1978.
[12] K. Tuber, D. Pocza, C. Hebling, Journal of Power Sources 124 (2003) 403–414.
[13] S. Litster, D. Sinton, N. Djilali, Journal of Power Sources 154 (2006) 95–105.
[14] A. Turhan, K. Heller, J.S. Brenizer, M.M. Mench, Journal of Power Sources 160 (2006) 1195–1203.
[15] X. Liu, H. Guo, F. Ye, C.F. Ma, Electrochimica Acta 52 (2007) 3607–3614.
[16] X.G. Yang, F.Y. Zhang, A.L. Lubawy, C.Y. Wang, Electrochemical and Solid State Letters 7 (2004) A408–A411.
[17] N. Pekula, K. Heller, P.A. Chuang, A. Turhan, M.M. Mench, J.S. Brenizer, K. Unlu, Nuclear Instruments & Methods in Physics Research Section A - Accelerators Spectrometers Detectors and Associated Equipment 542 (2005) 134–141.
[18] D. Kramer, E. Lehmann, G. Frei, P. Vontobel, A. Wokaun, G.G. Scherer, Nuclear Instruments & Methods in Physics Research Section A - Accelerators Spectrometers Detectors and Associated Equipment 542 (2005) 52–60.
[19] S. Shimpalee, J.W. Van Zee, International Journal of Hydrogen Energy 32 (2007) 842–856.
[20] V.P. Schulz, J. Becker, A. Wiegmann, P.P. Mukherjee, C.Y. Wang, Journal of the Electrochemical Society 154 (2007) B419–B426.
[21] S. Shimpalee, U. Beuscher, J.W. Van Zee, Journal of Power Sources 163 (2006) 480–489.
[22] P.P. Mukherjee, C.Y. Wang, Journal of the Electrochemical Society 153 (2006) A840–A849.
[23] H. Meng, C.Y. Wang, Journal of the Electrochemical Society 152 (2005) A1733–A1741.
[24] P.J. Culligan, K. Banno, D.A. Barry, T.S. Steenhuis, J.Y. Parlange, Journal of Geotechnical and Geoenvironmental Engineering 128 (2002) 327–337.
[25] D.A. DiCarlo, T.W.J. Bauters, C.J.G. Darnault, E. Wong, B.R. Bierck, T.S. Steenhuis, J.Y. Parlange, Journal of Contaminant Hydrology 41 (2000) 317–334.
[26] R.J. Glass, T.S. Steenhuis, J.Y. Parlange, Soil Science 148 (1989) 60–70.
[27] J.Y. Parlange, D.E. Hill, Soil Science 122 (1976) 236–239.
[28] T.W.J. Bauters, T.S. Steenhuis, D.A. DiCarlo, J.L. Nieber, L.W. Dekker, C.J. Ritsema, J.Y. Parlange, R. Haverkamp, Journal of Hydrology 231 (2000) 233–243.
[29] T.W.J. Bauters, D.A. DiCarlo, T.S. Steenhuis, J.Y. Parlange, Journal of Hydrology 231 (2000) 244–254.
[30] J. Selker, J.Y. Parlange, T.S. Steenhuis, Water Resources Research 28 (9) (1992) 2523–2528.
[31] Y. Liu, T.S. Steenhuis, J.-Y. Parlange, Journal of Hydrology 159 (1994) 187–195.
[32] Y. Liu, J.Y. Parlange, T.S. Steenhuis, Water Resources Research 31 (1995) 2263–2266.
[33] J.Y. Parlange, T.S. Steenhuis, R. Haverkamp, D.A. Barry, P.J. Culligan, W.L. Hogarth, M.B. Parlange, P. Ross, F. Stagnitti, Vadose Zone Hydrology - Cutting Across Disciplines (1999) 99–129 (Chapter 4).
[34] P.G. Saffman, G.I. Taylor, Proceedings of the Royal Society of London Series A 245 (1958).
[35] J.S. Selker, P. Leclerq, J.Y. Parlange, T.S. Steenhuis, Water Resources Research 28 (1992) 2513–2521.
[36] J.L. Nieber, T.W.J. Bauters, T.S. Steenhuis, J.Y. Parlange, Journal of Hydrology 231–232 (2000) 295–307.
[37] H.F. Nordhaug, M. Celia, H.K. Dahle, Advances in Water Resources 26 (2003) 1061–1074.
[38] J.Y. Parlange, W.L. Hogarth, Water Resources Research 21 (1985) 1283–1284.